8-2012

Synthesis and Applications of Novel Silver Nanoparticle Structures

Kyle Dukes
Clemson University, kdukes@clemson.edu

SYNTHESIS AND APPLICATIONS OF NOVEL SILVER NANOPARTICLE STRUCTURES

A Thesis
Presented to
the Graduate School of
Clemson University

In Partial Fulfillment
of the Requirements for the Degree
Master of Science
Chemistry

---

by
Kyle Dukes
August 2012

Accepted by:
Dr. George Chumanov, Committee Chair
Dr. Ken Christensen
Dr. William Pennington
Dr. Stephen Creager

ABSTRACT

The field of nanotechnology is rapidly expanding across disciplines as each new development is realized. New exciting technologies are being driven by advances in the application of nanotechnology; including biochemical, optical, and semiconductors research. This thesis will focus on the use of silver nanoparticles as optical labels on cells, methods of forming different small structures of silver nanoparticles, as well as the use of silver nanoparticles in the development of a photovoltaic cell.

Silver nanoparticles have been modified with self-assembled monolayers of hydroxyl-terminated long chain thiols and encapsulated with a silica shell. The resulting core-shell nanoparticles were used as optical labels for cell analysis using flow cytometry and microscopy. The excitation of plasmon resonances in nanoparticles results in strong depolarized scattering of visible light permitting detection at the single nanoparticle level. The nanoparticles were modified with neutravidin via epoxide-azide coupling chemistry and biotinylated antibodies targeting cell surface receptors were bound to the nanoparticle surface. The nanoparticle labels exhibited long-term stability under physiological conditions without aggregation or silver ion leaching. Labeled cells exhibited two orders of magnitude enhancement of the scattering intensity compared to unlabeled cells.

Dimers of silver nanoparticles have been fabricated by first immobilizing a monolayer of single silver nanoparticles onto poly(4-vinylpyridine) covered glass slides. The monolayer was then exposed to adenine, which has two amines which will bind to silver. The nanoparticle monolayer, now modified with adenine, is exposed to a second suspension of nanoparticles which will bind with the amine modified monolayer. Finally, a thin silica shell is formed about the structure via solgel chemistry to prevent dissolution or aggregation upon sonication/striping.

Circular arrays of silver nanoparticels are developed using a template base self assembly. A 1.5 micron silica sphere is bound to poly(4-vinylpyridine) coated glass and used as a template. a mask of silica monoxide is vacuum deposited atop the spheres/glass leaving a ring just below the sphere untouched and able to bind silver nanoparticles. Optical microscopy reveal interesting results under depolarized light conditions, but ultimate structural analysis has proven elusive.

Semiconducting p-type cuprous oxide was electrochemically deposited on both silver and indium tin oxide electrodes. Silver nanoparticles were incorporated into the architecture either atop the cuprous oxide or sandwiched between cuprous oxide and n-type material. Increases in photocurrent were observed in both cases and further work must be conducted to optimize a solid state device for photovoltaic applications.

DEDICATION

Foremost I must thank my wife, Sarah, for putting up with the seven day weeks, mood swings and general absence of her husband for close to four years. Sarah, you have the patience of a goddess. Next I feel compelled to thank Shire Pharmaceuticals, Cephalon, Roche and Sweetwater brewing company the makers of Adderall, Provigil, Klonopin and Sweetwater 420 respectively.

ACKNOWLEDGMENTS

I would like to acknowledge my fellow group members, past and present, for the advice, support and memories; John Heckel, Whitney Snyder, Zach Koontz, and Aubrie Pfirman. I would also like to thank my advisor Dr. Chumanov for all of his help through the years.

TABLE OF CONTENTS

LIST OF FIGURES

Figure Page

LIST OF TABLES

Figure Page

CHAPTER ONE

CORE-SHELL SILVER NANOPARTICLES AS OPTICAL LABELS

Introduction

Advances in the synthesis of nanoparticles have accelerated progress in developing new and robust methods of detection for bioanalytical applications.[1-3] The optical properties associated with plasmon resonances in metal nanoparticles (NPs), particularly silver and gold, are well-suited for optical labeling. The excitation of plasmon resonances, the collective oscillations of the conduction electrons, represents the most efficient mechanism for the interaction of light with matter.[4] Controlling the size, shape, and composition of metal NPs provides the possibility of tuning the plasmon resonances across the visible spectral range including regions where biological tissues have minimal light absorption.[4, 5] The excitation of plasmon resonances often results in strong resonant light scattering thereby facilitating optical detection of the particles.[4, 5] The scattering of light due to plasmon resonances in silver NPs is stronger than light scattering from the same size particles made of any other material.[6] This strong scattering allows high contrast imaging with little interference from the surrounding matrix.

Fluorescent labels are frequently used for cell-based assays and flow cytometry. However, limits of detection and overall sensitivity of fluorescence-based methods can be limited by cellular autofluorescence, quenching phenomena, photodecomposition, as well as transient blinking of fluorescent molecules.[6-8] Since metal NP-based detection methods are not limited by these phenomena, a variety of fluorescence-based biological assays have been

significantly improved by substituting metal NP labels.[8-11] Light scattering from gold NPs allowed 2-3 orders of magnitude improvement for detection of breast cancer cells.[12, 13] A two order of magnitude reduction in detection limit was also reported for other cell assays using metal NPs.[2, 6] Bioassays utilizing metal NPs enabled the detection of a single bacterial cell in less than one hour, significantly faster compared to other methods requiring amplification and/or complex detection schemes. [10, 12] Detection of antibody-antigen binding using nanoparticle-based optical labels also demonstrated single molecule sensitivity.[14] Nanoparticles have been also shown to be advantageous as labels for flow cytometry. [17] It was found that the incorporation of polymer NPs into the cells changes the average refractive index of the cytoplasm, thereby altering the side scattering of excitation light.[15] This change in refractive index was sufficiently large to distinguish cells loaded with NPs from cells that were NP free.[16] Metal nanoparticles, specifically Ag, Au, Cu have the additional benefit of the resonant interaction with incident light due to the excitation of plasmon resonances in the visible spectrum range.[17] Cell sorting has also been accomplished with magnetic nanoparticles,[18, 19] in which continuous and high-throughput separation of cells was achieved through the control of the magnetic field used to tune the velocity of cell flow.[20, 21] Both the velocity and the magnetophoretic mobility of the cells, typically labeled with a magnetic particle conjugated to a specific antibody of interest, was measured for differentiation.[21] This method of labeling overcomes the drawbacks associated with slow sorting rates and shearing in traditional fluorescence-based cell sorting.[18, 22] High-throughput screening has also been demonstrated in whole blood samples via core-shell gold NPs conjugated with specific antibodies for multi-antigen detection.[23] In this case, the gold NPs were designed to have

plasmon resonances in the NIR spectral range where hemoglobin and water do not absorb light to minimize potential interferences.

Changes of a plasmon resonance frequency were also used for monitoring binding of specific biomolecules via antibody conjugation.[24] Upon interaction with a specific ligand, such as a peptide, the surface plasmon resonance absorbance peak of the colloidal gold shifted toward longer wavelengths due to the increase of the local refractive index.[24] Successful application of metal NPs in biological systems largely depends on their stability in physiological conditions.[25] Gold has become the most common material used in biological systems because it is stable in physiological buffers and is biocompatible.[11, 13] Superior optical properties of silver NPs, specifically their larger-than-gold light scattering cross section, make them even more attractive for optical labeling.[26] However, Ag NPs have a tendency to aggregate in physiological buffers due the adsorption of chloride ions as well as exhibit cytotoxic effects.[5, 26, 27] Methods have been developed, with varying success, to stabilize the particles under physiological salt concentrations. These methods often include the formation of self assembled monolayers (SAM) on the surface of NPs or coating the NPs with surfactant molecules.[3, 26] These approaches are problematic for *ex-vivo* and *in-vivo* studies because the self-assembled and surfactant layers alone do not provide complete metal isolation due to possible ligand exchange taking place between adsorbed molecules on the surface of NPs and molecules present in systems under study. As a result, not only the stability on NPs is compromised, but leaching Ag ions cause toxic effects.[3, 27] Therefore, the development of nontoxic and stable Ag NPs would be an important addition to many biological applications involving optical labeling.

In this work, optical labels based on protected and surface-functionalized core-shell Ag NPs were developed and utilized for improving the detection of cells in flow cytometric and microscopic analysis due to the strong resonant light scattering associated with the plasmon resonances. The protection was achieved by a SAM providing a hydrophobic barrier on the metal surface for ions while the subsequent encapsulation of the NPs into a silica shell afforded stabilization of the SAM. The silica shell also provided a scaffold for nanoparticle functionalization via covalently linking neutravidin on the surface, a general strategy that can be used for a variety of biotinylated molecular recognition elements, including antibodies.

Experimental

Materials

Silver oxide (99.999% purity) was purchased from Alpha Aesar. (3-glycidoxypropyl)trimethoxy silane, tetramethoxysilane, biotin, bovine serum albumin (BSA), and EZ-link biotinylation kit were purchased from Gelest. 2-propanol (HPLC grade) and ammonia were obtained from VWR and were used as received. 11-mercapto-1-undecanol was purchased from Aldrich. Fluorescein and lyophilized neutravidin were obtained from Anaspec.

Instrumentation

Optical microscopy images were acquired with an Olympus IX71 inverted fluorescence microscope. Flow cytometry data were collected using a FACScan (Becton-Dickenson). Cytometry data were processed with FlowJo (Tree Star) software package.

Transmission electron microscopy was conducted using Hitachi H7600T electron microscope.

Synthesis of Ag NPs

Ag NPs were synthesized by the hydrogen reduction method previously developed in this laboratory.[5] Briefly, 0.25g silver oxide was added to 250mL 18Ω deionized water in a quartz reaction vessel. The vessel was pressurized with hydrogen gas (10 p.s.i) and heated to 70°C allowing the formation and growth of the NPs. The reaction was stopped by releasing hydrogen gas after the desired particle size was achieved. Particles with characteristic diameters of 90-100 nm were used in this work.

Synthesis and Functionalization of Core-Shell Ag NPs

Ag NPs were transferred into 15 mL 2-propanol and diluted to 1.5 optical density, as measured at the extinction maximum, followed by the addition of 0.05 mM 11-mercaptoundecanol in 2-propanol. The solution was mixed for 24h to allow the formation of the SAM. The observed 5 nm red-shift in the UV-Vis spectra confirmed the monolayer formation on the NP surface. The Ag NPs were encapsulated with silica via the sol-gel process. Briefly, 50uL of TEOS stock, 80uL ammonia, and 1.2mL 18 MΩ*cm deionized water was added to 15 mL of Ag NPs coated with the SAM in 2-propanol. The reaction was allowed to proceed overnight. Further treatment of the encapsulated NPs at temperature 125^{o}C further densified the glass shell as was determined from the slight blue shift of the plasmon resonance due to the shrinking of the shell. Core-shell Ag NPs were characterized

by UV-Vis Spectroscopy and TEM. Their stability was determined by monitoring UV-Vis extinction spectra of the particle suspension containing 1M NaCl over time.

Immobilization of Neutravidin

The surface of the functionalized Ag NP was modified with (3-Glycidoxypropyl) trimethoxysilane by the addition of 30 μL stock solution to 15mL modified Ag NPs in 2-propanol.[28] The vessel was stirred overnight followed by the centrifugation to remove the excess silane. After silanization, the epoxide was hydrolyzed to diol by addition of 50μL dilute sulfuric acid and allowed to stir for 2 hours. The diol was further oxidized to an aldehyde with addition of a solution consisting of 0.6mL water, 5.4mL glacial acetic acid and 0.1g periodic acid. The solution was stirred for 1 hour followed by centrifugation and resuspension in 2x PBS buffer. 2x PBS with 1 mg/mL BSA blocking buffer containing 0.2 mM EDC and 0.5 mM NHS was added to the solution and incubated for 15 minutes, followed by addition of 1 mg/mL neutravidin. The neutravidin-functionalized Ag NPs were centrifuged to remove excess protein and stored at 4^{o}C.

BSA labeled with fluorescein and biotin (FITC-BSA-biotin) and fluorescein directly conjugated to biocytin (FITC-biocytin) were added to the neutravidin-functionalized Ag NPs in 2x PBS buffer solution. The solution was lightly stirred for two hours and non-bound FITC-BSA-biotin conjugate was removed by washing and centrifugation. Solutions were used the same day or stored at 4^{o}C for no more than 4 days to maintain protein activity.

Cell labeling with core-shell Ag NPs

Fixed or live J774A.1 murine macrophage-like cells were exposed to biotin-conjugated rat anti-mouse IgG targeting the Fc cell-surface receptors. After a 30 min

incubation, the cells were washed free of unbound antibody and incubated with neutravidin-functionalized NPs. The strong binding affinity of neutravidin to biotin resulted in cell labeling with the Ag NPs.

Cell Culture

J774A.1 macrophage cells were cultured in T25 flasks in DMEM (Dulbecco's Modified Eagle's Medium) containing 10% fetal bovine serum, 1% penicillin-streptomycin and 1% glutamate and incubated in humidified environment (5% CO_2, 37 °C). The day prior to microscopy or flow cytometry, cells were plated at a density of 2×10^5 cells/dish in 35 mm glass bottom microscope dishes for microscopy or 35 mm petri dishes for flow cytometry and cultured overnight in DMEM + 10% FBS. Flow cytometry was carried out using standard methodology, in which the forward and side scattering channels were used for characterization. A minimum of 10,000 live or fixed cells were analyzed per run.

Results and Discussion

The combination of the self-assembled monolayer of long-chain alkane thiols and silica shell resulted in highly stable Ag NPs. These particles were exposed to 1M NaCl solution for several months and no changes in the UV-Vis spectra were noted during this time. The lack of the spectral changes indicated that the particles remained in their original non-aggregated state. Neither the silica shell nor the monolayer alone has shown comparable stability under the same conditions and in physiological solutions. The sol-gel silica shell is porous permitting chlorine ions to the Ag surface while the monolayer is subject to ligand exchange. The two together offer the best combination, in which the long alkane chain SAM provides the hydrophobic barrier for ions and the silica shell imparts chemical stability to the

hydrophobic barrier preventing ligand exchange. It was also noted that SAM-coated Ag NPs with a freshly synthesized silica shell did not exhibit the full stability in 1M NaCl solution. The full stability of the particles was acquired after several days of shelf-storage, which was attributed to continuing densification of the sol-gel silica. Alternatively, heat treatment of the core-shell NPs in a sealed Teflon reactor at ca. 125°C for a few hours produced fully stable particles. The integrity of the silica shell after the exposure to 1M NaCl was confirmed by electron microscopy revealing the original 20 nm thick layer around Ag NPs (Figure 1).

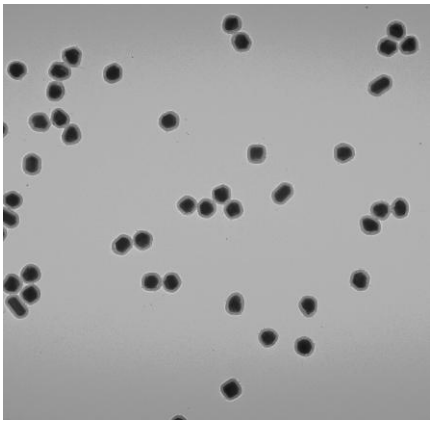

Figure 1. TEM image of SAM coated Ag NPs with silica sol-gel shells after exposure to 1M NaCl solution for 14 days.

The silica shell also provides a convenient scaffold for surface modifications via silane chemistry for the attachment of biomolecules. Immobilization of neutravidin was achieved via epoxide coupling chemistry that produced a NHS linker on the surface of the NPs (Scheme 1). [28]

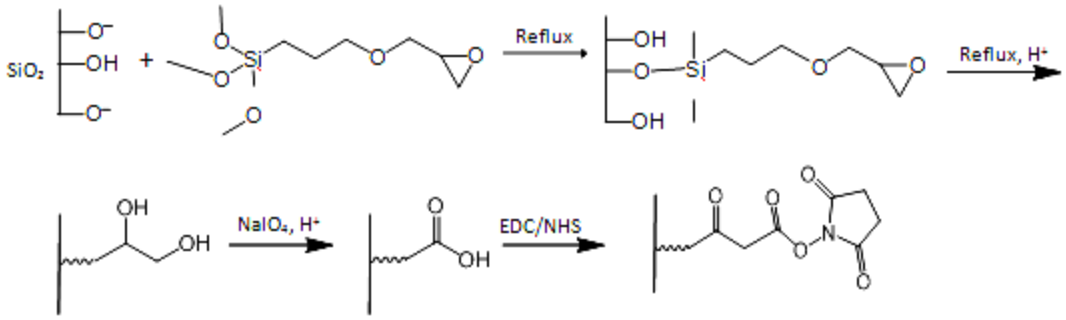

Scheme 1. Surface modification of core-shell Ag NPs for attaching proteins.

Biotin-fluorescein conjugates and FITC-BSA-biotin were used to verify the presence of neutravidin to the surface of the NPs. The NPs were exposed to either conjugate and, after extensive washing, were examined by fluorescence microscopy. Fluorescence was observed in both cases indicating the presence of neutravidin on the surface of the NPs as well as confirming that biotinylated proteins can be attached to the surface of the NPs via this route (Fig. 2). No fluorescence was detected from core-shell Ag NPs without the neutravidin modification when exposed to biotin-fluorescein conjugates and FITC-BSA-biotin indicating little or no nonspecific binding to the silica shell. Protected core-shell Ag NPs with surface immobilized neutravidin constitute advanced optical labels for *ex vivo* labeling under physiological conditions. They provide easy detection due to the large light scattering cross section associated with plasmon resonances as well as broad utility for conjugating to various biomolecules through the biotin linker.

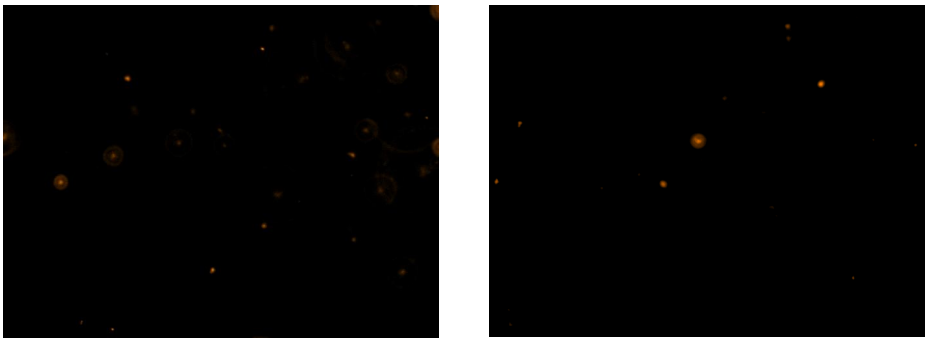

Figure 2. Fluorescence images of core-shell Ag NPs with immobilized neutravidin and exposed to a) FITS-BSA-biotin and b) FITS-biotin. Microscope objective: 60x oil immersion. The apparent hallo around some particles is due to particles being out of focus.

In order to demonstrate the utility of the core-shell Ag NPs as biological labels, the NPs were attached to the surface of live cells and cells were imaged with the microscope using two crossed polarizers. The crossed polarizers provided a superior observation method, because they block transmitted light rendering the background dark. At the same time, the nanoparticles appear bright due to their ability to depolarize scattered light that has a polarization component orthogonal to the polarization of incident light, while cells and surrounding matrix do not significantly depolarize light. Plasmonic NPs depolarize scattered light due to their nonspherical shape that results in the excitation of at least two plasmon modes (along different axes of the particle) with different but overlapping frequencies.[29] When excited with the frequency in the spectral region where the two modes overlap, the two simultaneously excited modes will be out of phase and undergo interference resulting in the induced particle polarizability with the component perpendicular to the polarization of the incident light. This perpendicular component is the origin of the depolarized scattering that is observed through the two cross polarizers.

Images of unlabeled and core-shell Ag NP-labeled cells obtained in transmitted light mode through a polarizer-analyzer pair are shown in Fig. 3. When the polarization axes of

the polarizer and the analyzer were parallel to each other, the labeled (Fig. 3a) and unlabeled (Fig. 3d) cells appeared similar and no Ag NPs were seen. At nearly cross-polarized geometry, when the polarization axis of the polarizer and analyzer were not quite orthogonal, the unlabeled cells still could be seen but the image had a low signal-to-noise ratio as is evident from the grainy appearance of the background (Fig. 3e). At the same time, the labeled cells appeared with bright nanoparticle labels (Fig. 3b). When the polarizer and analyzer were completely crossed, the unlabeled cells could not be observed (Fig. 3f) while the labeled cells were unmistakably identified by bright depolarized scattering from the Ag NPs on the dark background (Fig. 3c). In addition, some cell features can also be seen in the cross polarized geometry likely due to the secondary illumination by light scattered from the Ag NPs.

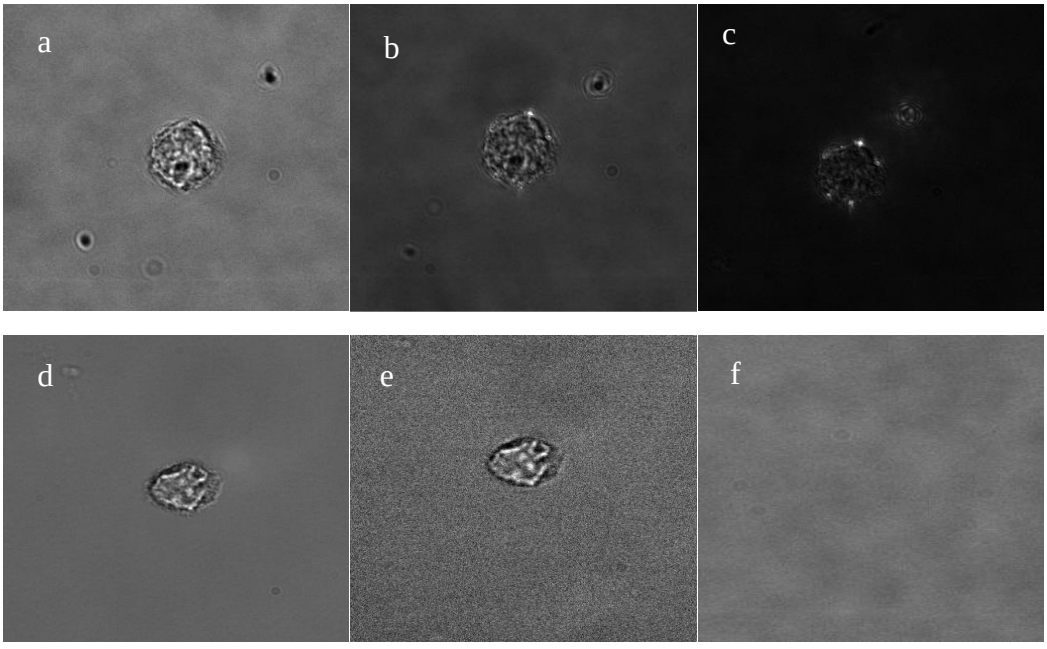

Figure 3. Cells viewed in polarized light through: (a, d) an analyzer oriented parallel to the polarizer; (b, e) an analyzer nearly crossed relative to the polarizer; (c, f) an analyzer at 90° to the polarizer. A cell labeled with core-shell Ag NPs (a-c) and a cell without core-shell Ag NPs (d-f). Note that the unlabeled cell is invisible in (f) whereas core-shell Ag NPs attached to the cell are clearly seen under the same conditions in (c).

As Ag NPs show strong light scattering, we expected that these functionalized particles could be used as scattering labels in flow cytometry as opposed to typical fluorescent staining. Live or fixed J774A.1 cells were labeled with the stabilized neutravidin conjugated core-shell Ag NPs and analyzed in the flow cytometer with the forward and side scattering channels (488nm excitation). The analysis of flow cytometry histograms from the labeled and unlabeled cells showed approximately two orders of magnitude increase in scattering intensities for core-shell Ag NP labeled cells in the side scatter channel (Fig. 4). At the same time, the distribution of the intensities for the population of the labeled cells was also broader, most likely reflecting the distribution of the number of the labels per cell. Indeed, the average number of Ag NP labels per cell varied from 6 to 20 although cells with as few as one NP and as many as ca. 30 were also observed (data not shown).

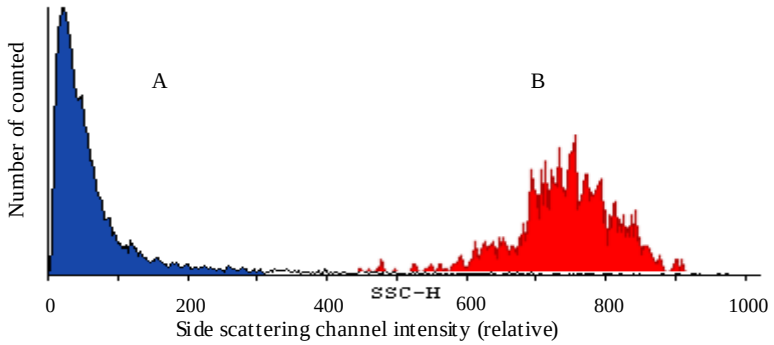

Figure 4. Flow cytometric profile of (a) nonlabeled cells and (b) cells labeled with core-shell Ag NPs.

Conclusion

Core-shell Ag NPs modified with long chain thiols and encapsulated into a thin silica layer acquire long term stability in physiological salt conditions. This stability and the presence of a plasmon resonance that manifests itself as strong resonance light scattering present an opportunity for optical labeling in bioanalytical applications using only scattering. The outer silica shell provides a scaffold for surface modifications, as shown here with neutravidin, which suggests this is a platform method for attaching biomolecules to the Ag NPs as labels for flow cytometry and in polarized light microscopy. The ability of aspherical plasmonic particles to depolarize scattered light allows simple and efficient means for elimination of background by observing particles through crossed polarizers. [29] The application of core-shell plasmonic particles as optical labels was demonstrated for analysis using flow cytometry where an increase of two orders of magnitude in the side-scatter intensity was observed and could be used to differentiate the two populations. Strong light scattering from core-shell Ag NPs permits the discrimination of individual NP labels and opens the potential for distinguishing small differences in composition of cell membrane.

CHAPTER TWO

FORMATION AND STABILIZATION OF NANOPARTICLE DIMERS FOR OPTICAL STUDIES

Introduction

Nanostructures comprised of several NPs very near each other exhibit different Plasmon field effects than a single NP. The scattering and plasmonic coupling of NPs in these assemblies have interesting properties and applications in labeling, surface-enhanced Raman spectroscopy (SERS), optical data storage, energy transport, optical waveguides[4] etc. The interaction of NPs with visible light is polarization dependent, and this effect has been modeled by simulation and in spectroscopic studies. Recently, our lab has been interested in the depolarized scattering exhibited by asymmetrical silver NPs. Single NPs of differing aspect ratios were studied exhaustively; with the results suggesting that depolarized light scattering is strongest for NPs with the largest aspect ratio. The natural progression of this work is to study this phenomenon in small clusters of NPs, specifically dimers and trimers. A method to prepare such structures, which are stable over periods of weeks at minimum, is needed to probe these structures.

In general, methods to produce small clusters of NPs have been sought for quite some time in order to study near-field plasmonic interactions. The ability of small clusters of nanoparticles to focus electromagnetic radiation has been studied and modeled, with potential use in sensing applications such as surface-enhanced Raman spectroscopy. Reproducibility is a problem with most published methods at best yielding

only 60% of a single species (dimers, trimers) often with the aid of a separation/isolation step. In addition, some of the most reliable and reproducible methods use long linking molecules. Physical separation of the nanoparticles by more than a few nanometers retards the plasmonic coupling between them, making them non-ideal for such studies. For spectroscopic studies, as well as the chemically clean nature of the nanoparticles used, filtration introduces potential for contamination or aggregation. Therefore a method was developed to first immobilize single NPs, link a second NP via small molecule, and encapsulate the dimer in a thin silica shell to prevent further olglomerization. This method has an advantage over a solution phase approach because the immobilized NP have less surface area exposed for modification with linkers thereby reducing the likelihood of multiple NPs binding and causing aggregation.

Linking methods which have been used in the past include condensation of carboxyl and amine functional groups bound to NPs via thiol linkage. [30] This method requires the formation of a SAMs containing these functional groups in two separate suspensions of NPs and EDC/NHS linking chemistry. The method suffers two drawbacks, specifically high salt concentration in the buffer that causes aggregation and low yield of dimers (20%<). Dithiols have been also used; [30] with nearly identical results as the condensation reaction in solution, and with a little bit little better results when NPs were immobilized on surfaces.

Experimental

To create a single NP monolayer on glass, a slide is placed in a 0.01% solution of poly(vinylpyridine) (PVP) in ethanol for several hours. The PVP-modified slide is rinsed

thoroughly with ethanol and dionized water, followed by immersion into an aqueous solution of silver NPs. Monolayers are formed upon the glass substrates within a few hours as the NPs bond to the PVP amine groups. Adenine was chosen as a linker molecule because it has two amine groups which can bond with silver NPs. The NP monolayers were washed thoroughly with water and treated with adenine for several hours. The resulting NP monolayer with bound adenine is again placed into a solution of silver NPs for several hours and washed with dionized water. Ultrasonication is required to remove the NP dimer structures from the PVP coated slide. In order to strip the NP dimmers while keeping the structure intact, a thin (~10nm) silica shell is coated around the NPs via sol-gel silane chemistry. Briefly, adenine modified NP monolayers are placed in custom-made cassettes filled with alcohol solution (ethanol or propanol). To the solution 100mL of water is added, followed by the rapid addition (seconds) and mixing of 80 µL ammonia, and 100 µL of a .01% solution of tetraethyl orthosilicate (TEOS). The cassettes are sealed and allowed to mix for 48 hours, after which they are washed generously with alcohol and deionized water.

Results and Discussion

Several different linker molecules were tested for this project with mixed success. Adinene was ultimately chosen because the dimers formed were by far the most stable and reproducible. Table 1 summarizes other linker molecules used and the resulting composition of the NPs. Linking molecules were chosen based upon the following criteria; size, the presence of two attachment sites, and chemical stability towards NPs

and solvent. It was found that many linkers, such as the dithiol, promoted nanoparticle aggregation. This aggregation occurred in solution as well as on the surface. Reducing concentration and exposure time had little to no effect on the stability. Adenine was found to be the most reproducible and further studies on alternative linkers were ceased.

Molecule	Concentration (total)	Phase	Solvent	Result
1,9 dithiol	1.0×10^{-4} M	Soln.	Ethanol	Aggregation
1,9 dithiol	1.0×10^{-4} M	Monolayer	Ethanol	Aggregation
11-MBA*	1.0×10^{-4} M	Soln.	Ethanol	Aggregation
11-MBA*	1.0×10^{-4} M	Monolayer	Propanol	Aggregation
11- amine**	1.0×10^{-4} M	Soln.	Ethanol	Aggregation
1,9 dithiol (10%) 1,9 nonanethiol (90%)	1.0×10^{-4} M	Soln.	Ethanol	Aggregation, few dimers
1,9 dithiol (1%) 1,9 nonanethiol (99%)	1.0×10^{-4} M	Soln.	Ethanol	Aggregation, some dimers

Table 1. Different linker molecules used in dimer studies. *mercaptoundecanoic acid, ** 11-Amino-1-undecanethiol

The resulting thin silica shell is sufficient to keep the NP structure intact and thin enough so as not to prevent stripping of the NP dimers (figure 5). The criteria most critical to the successful stripping of the structure was the TEOS concentration, if the concentration was too high the shell thickness was sufficiently thick as to bind the structure to the slide. If the concentration to low, the dimmers were unstable after sonication. This method produces between 40-60% dimers with few large aggregates. The dimers were used by a fellow group member to study depolarized light scattering by the structures.

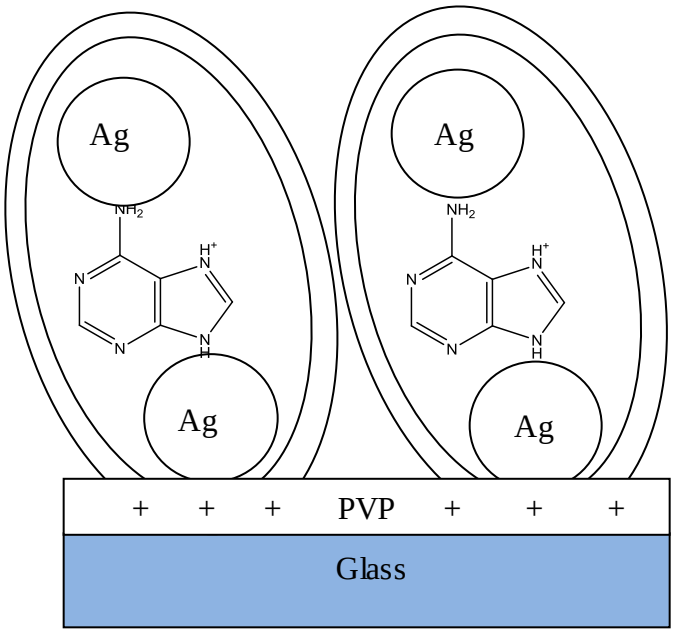

Figure5: Illustration of NP dimers formed through modification of a NP monolayer with adenine, followed by silica encapsulation. The thin silica shell stabilizes the dimer and prevents aggregation during stripping.

CHAPTER THREE

TEMPLATED SELF ASSEMBLY OF SILVER NANOPARTICLES

Introduction

Metal nanoparticles have strong and unique optical resonances in the visible and near-infrared (NIR) region of the electromagnetic spectrum due to resonance of their free electrons to the electric field of light. [30] When a metallic nanoparticle is subject to light excitation, the electric field of the light induces waves of collective electron oscillations confined to the surface of the nanoparticle, a phenomenon known as a localized surface plasmon resonance (LSPR).[31] The surface plasmon oscillations induced by the field of the light result in a strong electric field confined to the surface of the nanoparticle. Due to the strong resonance, this near-field is enhanced on the surface of the nanoparticle relative to the incident field E_0 at frequencies corresponding to the LSPR. The electric field E at the surface of a metal nanoparticle is given in the dipolar limit by [31]

$$E_{surface} = \frac{(1+\kappa)\varepsilon_m}{(\varepsilon+\kappa\varepsilon_m)}E_0$$

Where κ corresponds to the geometry of the particle and ε represents dielectric medium surrounding the particle. The strong plasmonic near-field greatly enhances the electronic transitions of optical absorbers and emitters (resonant with the LSPR frequency) placed

in the vicinity of the nanoparticle. A example of such a plasmonic near-field enhanced process is surface-enhanced Raman scattering (SERS)

When two metal nanoparticles are brought in close proximity to each other, the near-field on one nanoparticle can interact with that on the other particle.[30] Due to this interaction, the electric field E felt by each particle is the sum of the incident light field E_0 and the near-field E_{nf} of the neighboring particle. The result is the coupling of plasmon resonances between the particles and this coupling dictates the LSPR frequency of the coupled nanoparticle system. [30] The concentration of surface plasmons at the interface of the NPs generates high energy local "hot spots" between the interacting particles (Figure 6). Plasmonic coupling between more than two NPs, in different geometries and sizes, has been studied as well and is of great practical interest in techniques such as SERS.

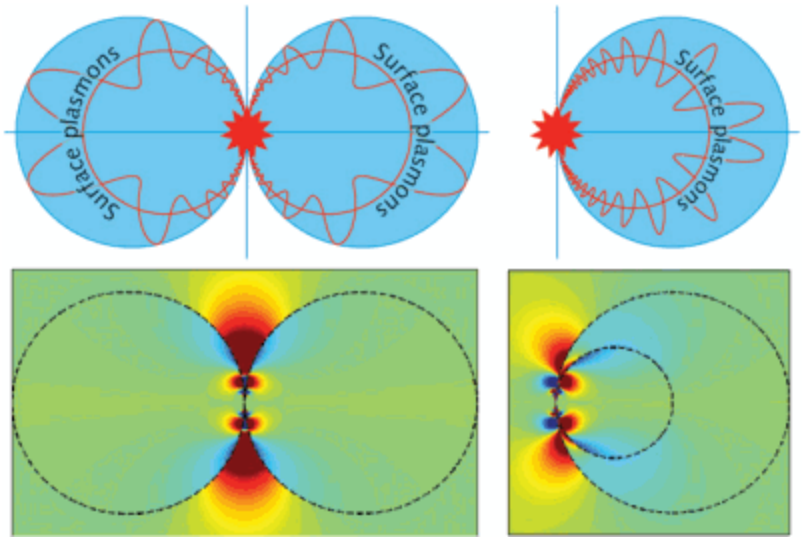

Figure 6: Plasmon coupling between two nanoparticles (left) and single nanoparticle Plasmon resonance(right)

Arrays of plasmonic NPs exhibit a wide range of optical and electrical properties. Plasmon resonances in NP arrays respond to change in the surrounding dielectric environment, a response which may be exploited for use in sensing platforms for chemical or biological systems. In addition, the shape, size, and relative particle to particle distance of NPs and NP arrays dictate the spectral signature of the Plasmon resonance and the relative sensitivity to changes in the surrounding dielectric medium.[30] [32] This allows for tunable sensing platforms, as has been demonstrated by the work of Van Duyne and many others in the field. [32, 33] NP arrays have been successfully used in many biological and chemical applications, including the detection of proteins, antibody-antigen interaction, surface enhanced raman spectroscopy (SERS). In a recent example, nanoparticle cluster arrays (NCA's), small clusters of 3-6 NPs in a roughly triangular pattern were used in SERS detection of TNT contaminate 2,4-dinitrotoluol (DNT) and demonstrated a sensitivity of 10 ppt.[34] [34] The NCA's used in the experiment were fabricated using a lithographic method and highlight the utility of plasmonic structures in important sensing applications. One drawback in using lithography in fabrication of plasmonic structures is the (often) high cost and limited scalability. A simple, scalable, and inexpensive method of generating new NP arrays would be of great practical significance.

In this work, micron sized silica beads were used as a template for silver NPs to be arranged, forming a circular array. This was achieved by depositing the silica beads on a PVP modified glass slide (described earlier), followed by vacuum deposition of a silica monoxide mask. The silica monoxide covered the surface of the modified glass except

the region directly under the silica beads acting as a mask (shaded green Figure 7). Using this technique the diameter of the circular arrays, and therefore number and size of the plasmonic structure, can be tuned by varying the size of the template sphere.

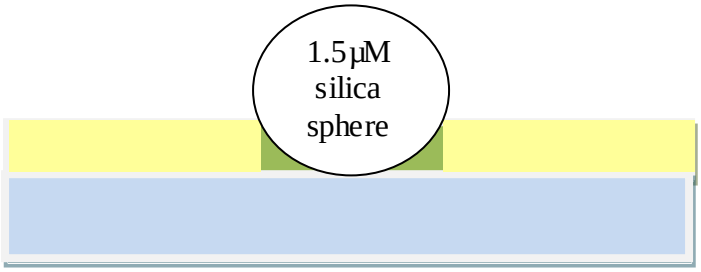

Figure 7: Schematic of template used for self assembly of circular NP arrays. The green area under the silica bead indicates the remaining PVP modified glass surface for NPs to bind

Experimental

Micron-sized silica beads were used as a template for silver NPs to be arranged, forming a circular array. This was achieved by depositing the silica beads on a PVP modified glass slide (described earlier), followed by vacuum deposition of a silica monoxide mask. The silica monoxide will cover the surface of the modified glass except the region directly under the silica beads, which acts as a mask (shaded green Figure 6). A polymer-modified slide is placed in an acidic aqueous solution containing 1.5 micron silica beads. Lowering the pH was necessary for the beads to bind to the PVP modified slide. This is due to hydrogen bonding between silica surface (pKa 4-5) and the pryidal group in PVP (pKa~4). The modified slides are cleaned and placed in a vacuum

deposition chamber where 20-100nm of silicon monoxide is vapor deposited. The slides are then immersed in a solution of silver NPs for several hours.

Results and Discussion

Optical microscopy with polarizers crossed at the light source and detector reveal a cross-like pattern of brightly colored nanoparticles. The intensity of the depolarized scattering from the NPs is dependent on the position of the NP relative to the polarization of incident illumination. For an immobilized particle this means that rotating the polarizers, while maintaining orthogonal vectors, will result in the intensity of the scattered light modulating. Figure 8 shows silica beads prior to exposure to NPs illuminated with varying degrees of polarized light. Figure 9 shows the same substrate after immersion in NPs with the same varying degree of polarization.

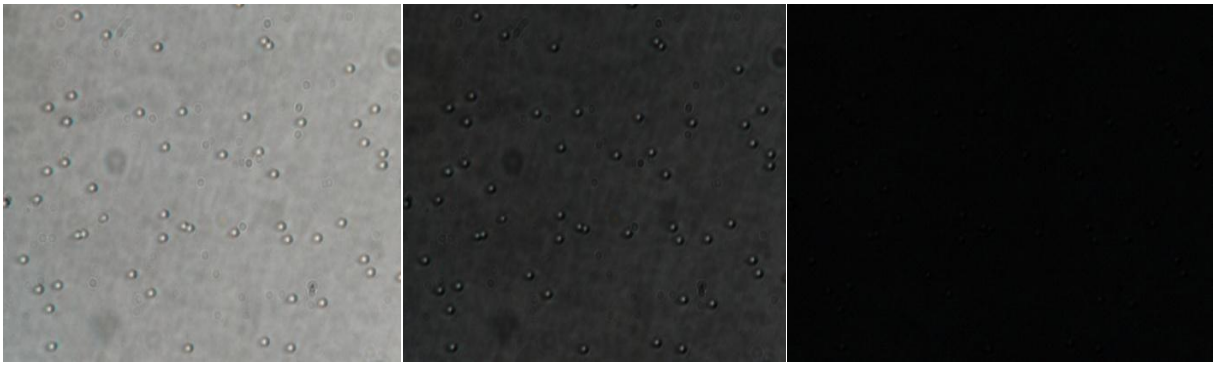

Figure 8: Silica beads prior to exposure to NPs under normal illumination b) nearly crossed polarized illumination, and c) crossed polarized illumination

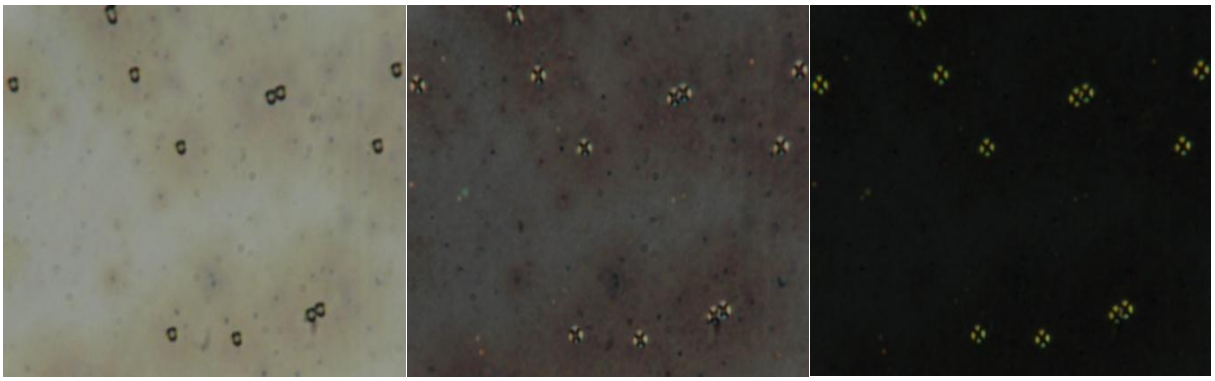

Figure 9: Silica beads after exposure to silver NPs under normal illumination b) nearly crossed polarized illumination, and c) crossed polarized illumination

Attempts were made to characterize the substrates by atomic force microscopy and electron microscopy. Ultimately little evidence was attained as to the actual structure of the NP array because the NPs are effectively buried under the side of larger silica sphere. Larger polystyrene (PS) beads were used (25 micron) and yielded the best

evidence of a circular NP array. The refractive index of the polystyrene spheres nearly matched that of the oil immersion microscope and NP could be directly visualized as the polystyrene was nearly transparent. Electron microscopy revealed a dense circular array of an area in which the polystyrene bead broke away from the substrate, leaving behind the bound NPs (Figure 10). The NP arrays were quite thick and symmetric with template spheres in place and asymmetrical at points where template spheres were absent. This is likely due to some NPs stripping off with the template sphere.

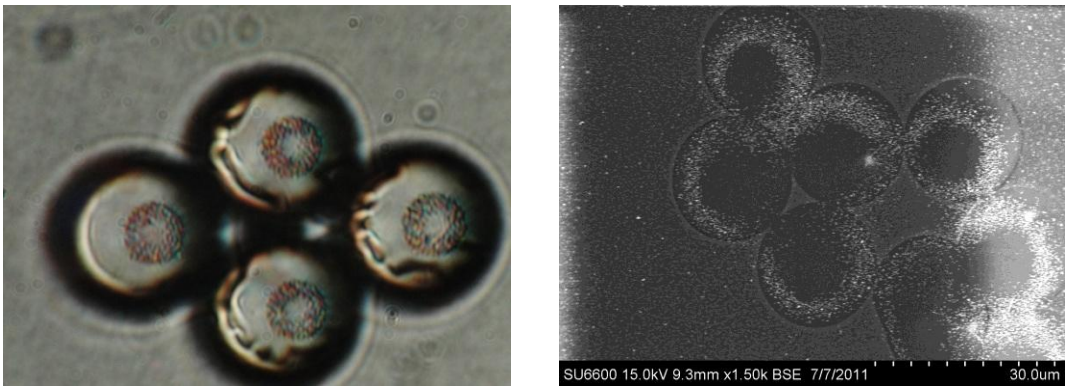

Figure 10: Optical microscope (100x oil immersion) image of 25micron PS beads with circular NP pattern and b) electron microscopy of an area of the template in which PS beads were removed

Conclusion

Visualizing NPs formed around the smaller 1.5 micron silica beads via electron microscopy was not possible and characterizing with atomic force microscopy did not yield structural information. Due to the geometry of the structures it was likely the NPs

were buried and surface analysis proved inconclusive. The smaller arrays were ultimately abandoned because of the lack of structural information. Although reproducible, without detailed structural information the star-like patterns observed via optical microscopy could not be conclusively identified. The use of larger template beads yielded structures which could be characterized optically and via surface analysis, but consisted of a dense ring of NPs. Although these structures could have some interesting applications, the goal of achieving arrays of single NPs was not achieved.

CHAPTER FOUR

PLASMONIC CUPROUS OXIDE- SILVER NANOPARTICLE PHOTODIODE

Introduction

Increasing worldwide energy demands coupled with increasing fuel prices have created a large demand for more affordable and sustainable energy.[15] Fossil fuel sources are finite and damage the environment. Nuclear power has inherent danger associated with its use as well as producing hazardous waste material. Currently there is a push for development of more efficient and clean energy sources, as well as improving existing technologies. Solar cells, which are sustainable, clean, and safe have been a steadily growing technology for decades. Increasing efficiencies in solar cells make their use more economical and, with sufficient gains, may replace fossil fuels.[15] Aside from the traditional silicon based solar cells, many designs depend upon rare and sometimes toxic materials. Development of a photovoltaic cell with abundant and safe materials that can match the output of current solar technologies is a highly sought after technology.

Copper oxide is one of the oldest studied materials which exhibit photocurrent.[22] Cuprous oxide (Cu_2O) is a p-type semiconducting material with a bandgap around 2.0 eV.[23] Its high optical absorption coefficient in the visible range and reasonably good electrical properties make it an appealing candidate for use in the design architecture of a photovoltaic device. The most efficient photovoltaic device constructed with cuprous oxide is 2% efficient, far below current silicon and gallium arsenide devices.[24] Methods

to improve the efficiency of cuprous oxide devices are needed in order for it to become a viable material for use in solar cells. A method which has not been explored is the use of plasmonic NPs to increase the efficiency of cuprous-oxide-based devices in solar energy conversion.

Properly engineered metal structures - called plasmonics - can localize incident light on a sub-micrometric scale and could therefore be used to enhance solar light absorption in ultrathin semiconductor films.[25-27] Plasmonic nanoparticles can be tuned in size and shape to interact with a specific range of visible light, allowing tuning for a particular semiconducting materials bandgap and therefore may be used to maximize collection (absorption) in a semiconducting film.[25] In addition, because of the multiple and high-angle light scattering characteristic of plasmonic NPs the effective film thickness is increased, allowing for thinner films with the same efficiency (Figure 11).[15] By dramatically reducing the required thickness of the active layer, the use of plasmonics is expected to expand the range and quality of absorber materials that are suitable for photovoltaic devices.[14,15] In particular, this would enable effective utilization of both low-dimensional semiconductor structures and thin films of earth-abundant, low-cost, and non-toxic absorbers with poor charge transport properties.[15,27] Cuprous oxide is one such material which has not been focused upon in current plasmonic photovoltaic and solar cell development. The main body of literature on the subject focuses on current technologies based on silicon, gallium arsenide, and organic photodiodes. The goal of this project is to increase the efficiency of cuprous-oxide-based photovoltaics by

optimizing deposition conditions, contact material, and increasing the adsorption of the thin film by incorporating silver NPs

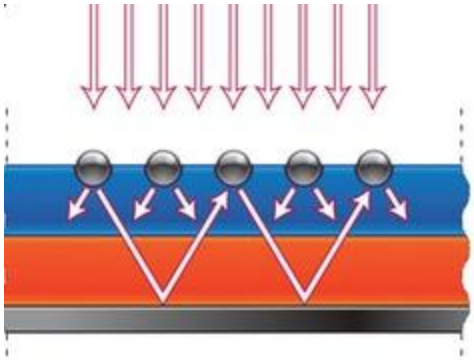

Figure 11: Light trapping by scattering from NPs at the surface of a solar cell. Light is preferentially scattered and trapped into the semiconductor thin film by multiple and high-angle scattering, causing an increase in the effective optical path length in the cell[15]

Preliminary experiments have been conducted utilizing electrochemically deposited cuprous oxide films on both silver films and ITO glass. Electrochemical deposition is appealing because it is an easily scalable and relatively low cost method of producing semiconducting films.

Experimental

Silver electrodes were fabricated on clean glass substrates by vacuum deposition of the metal. Due to poor silver adhesion, a thin (~20nm) underlayer of chromium was first deposited followed by the deposition of 150nm silver. ITO (100 Ω) glass was used as received. The electrolyte for electrochemical deposition of cuprous oxide was made of a 0.4M solution of copper sulfate and 3M lactic acid, adjusted to pH 9.8 with sodium hydroxide. The lactic acid acts as a complexation agent for copper ions. Cuprous oxide

was electrodeposited by reduction of an alkaline aqueous solution of cupric lactate according to the reaction:

$$2Cu^{2+} + 2e^{-} + 2OH^{-} \longrightarrow Cu_2O + H_2O$$

The deposition potential was held at -0.35V v/s saturated Ag/AgCl reference electrode. Platinum foil in a form of a ring was used as the counter electrode. Depositions were carried out with a CHI 400a Electrochemical Workstation (CH Instruments) until the total charge reached 0.02-0.06 coulombs depending upon the desired film thickness. Figure 12 is a picture of the electrochemical cell used for the deposition of cuprous oxide and its electrochemical characterization.

Figure 12: Electrochemical cell with Teflon cap, platinum foil auxiliary electrode, and saturated Ag/AgCl reference

Control of pH is critical for the formation of cuprous oxide, as at neutral and acidic pH copper is obtained via the reaction:

$$2Cu^{2+} + 2e^{-} + 2H^{+} \longrightarrow 2Cu + H_2O$$

Light yellow cuprous oxide films were characterized electrochemically and by UV-Vis spectroscopy. Electrochemical characterization was carried out in 1.0mM sodium sulfate

unless otherwise specified. The cuprous oxide films were excited using a 150 watt halogen lamp coupled into a fiber and recorded with CHI acquisition software. A typical photoresponse of a cuprous oxide film on the silver working electrode is shown in Figure 13, where the cathodic current indicates p-type semiconducting behavior

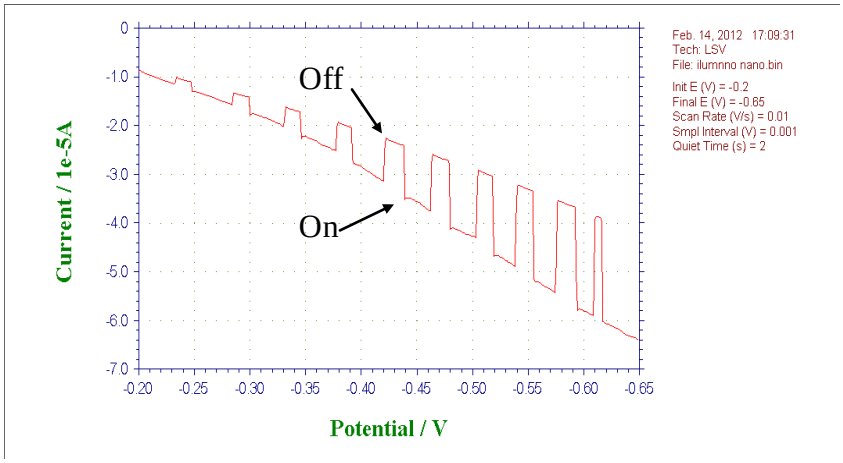

Figure 13: Photoresponse characterization of Cu_2O films deposited electrochemically at 0.035V, pH 9.8 and total charge equal to 0.02 coulombs. The potential scan was from -0.2v - -0.65v at 0.01v/s with chopped illumination.

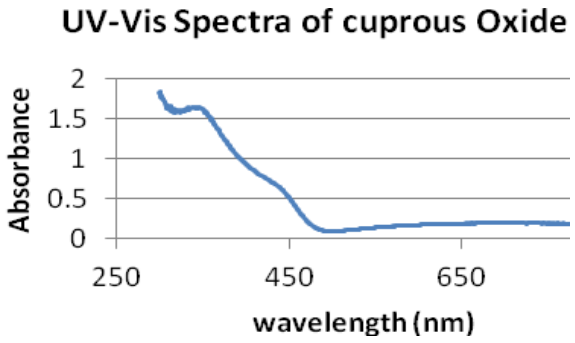

Figure 14: UV-Vis absorbance spectra of cuprous oxide

Results and Discussion

Electrochemical deposition of cuprous oxide is known to form first a very thin (few nm) copper layer before oxygen is inserted into the lattice.[16] This copper-cuprous oxide contact is considered a Schottky contact due to the differences in workfunction. The copper-silver contact is ohmic in nature, so the Mott-Schottky relationship may be used for electrochemical characterization. In order to calculate the flatband potential and carrier concentration, Mott–Schottky (MS) plots were generated from impedance measurements. A MS plot of ($1/C^2$ vs. E) allows for the donor density to be calculated from the slope (s), and the flatband potential can be determined by the intercept (V_0).[14] The MS relationship is given by:

$$\frac{1}{C_{CS}^2} = \frac{2}{\varepsilon\varepsilon_0 eN}\left(E - E_{fb} - \frac{kT}{e}\right) \quad (1)$$

Where C_{SC} is the charge space capacity, N the carrier density, ε the relative electric permittivity, ε_0 the electric permittivity of vacuum, e the elementary charge, k the Boltzman constant, T the absolute temperature, E_{fb} the flat band potential and E is the potential.

Extrapolating from (1)

$$N = \frac{2}{e\epsilon\epsilon_0 A^2 S} \quad (2)$$

And

$$E_{fb} = V_0 + \frac{KT}{e} \quad (3)$$

At room temperature the value kT/e is 0.026eV and is commonly considered negligible.[13] Figure 15 is a MS plot of the above cuprous oxide film. According to the intercept the flatband potential is – 0.2Vwhich is in agreement with the literature.[35] Charge carrier density is calculated from the slope to be 5.4 x 10^{18} cm^{-3}.

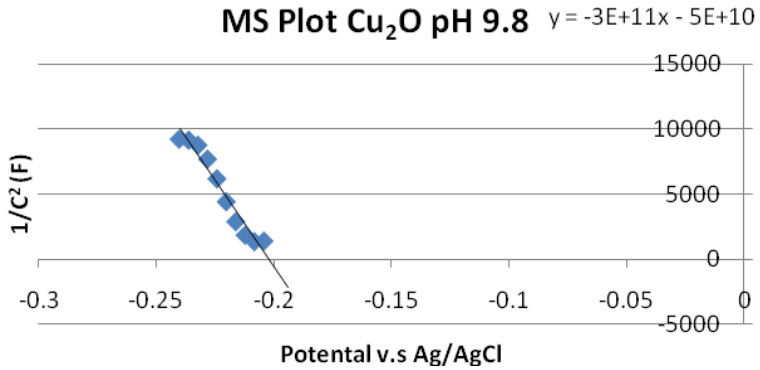

Figure 15: MS plot for cuprous oxide films electrochemically deposited on silver films

This preliminary work will provide the foundation for fabrication of devices centered around metal semiconductor contact between silver and cuprous oxide. N-type materials

which can also be deposited electrochemically, such as zinc oxide, are being explored as absorber materials to form a p-n junction. The focus however, will be on incorporating plasmonic NPs into these devices with the goal of improving performance. Insulating materials will need to be explored to prevent short circuiting, and device architecture (film thicknesses, possible dopants) will need to be carefully optimized.

CHAPTER FIVE

CONCLUSION

Silver NPs are extensively studied due to their optical properties stemming from excitation of plasmon resonances and practical use as optical labels. Core shell silver NPs were synthesized and successfully modified to bind to cells for use as optical labels and in flow cytometry. The formation of dimeric silver NPs for fundamental optical studies was successfully carried out using an adenine linker and silica encapsulation. These dimers may also be useful in both surface enhanced Raman scattering experiments and enhanced fluorescence. Templated circular arrays of silver NPs were fabricated, demonstrating interesting optical properties, but ultimately characterizing the precise structure of desired, single NP wide circles, could not be obtained. Cuprous oxide films have been electrochemically deposited on silver films and characterized as p-type semiconducting material. Fabrication of a photovoltaic device will be continued, with ideal absorber (n-type) materials studied and through incorporation of plasmonic NPs. A photovoltaic device made up of safe and abundant materials, which is also easily fabricated and is scalable, may prove to be an alternative route for fabrication of clean energy devices.

References

1. Prasad, P., Polymer science and technology for new generation photonics and biophotonics. *Current Opinion in Solid State and Materials Science* **2004,** *8*, 11–19.
2. Sharma, P., Nanoparticles for bioimaging. *Advances in Colloid and Interface Science* **2006,** *123-126*, 471-485; Selvan, S., Functional and Multifunctional Nanoparticles for Bioimaging and Biosensing. *Langmur* **2009**.
3. Mallander, V. L., K, Interaction of Nanoparticles with Cells. *Biomacromolecules* **2009,** *10*, 2379-2400.
4. Kreibig, U. V., M., *Optical Properties of Metal Clusters*. Springer-Verlag: New York, 1995; Vol. 25.
5. Evanoff, D. C., G., Size-Controlled Synthesis of Nanoparticles. 2. Measurement of Extinction, Scattering, and Absorption Cross Sections. *The Journal of Physical Chemistry B* **2004,** *108* (37), 13957-13962.
6. Jian Zhang, Y. F., Dong Liang, Richard Y. Zhao, and Joseph R. Lakowicz, Fluorescent Avidin-Bound Silver Particle: A Strategy for Single Target Molecule Detection on a Cell Membrane. *Analytical Chemistry* **2009,** *81* (3).
7. Venkatachalam, N. O., Y., Bioimaging of M1 Cells Using Ceramic Nanophosphors:
Synthesis and Toxicity Assay of Y2O3 Nanoparticles. *Journal of Physics: Conference Series 191 (2009) 012002* **2009**.
8. Yong, K. S., M. T.; Ding, H., Preparation of Gold Nanoparticles and their Applications in Anisotropic Nanoparticle Synthesis and Bioimaging. *Plasmonics* **2009,** *4*, 79-93.
9. Seydack, M., Nanoparticle labels in immunosensing using optical detection methods. *Biosensors and Bioelectronics* **2005,** *20*, 2454-2469; Selvan, S. T.; Tan, T. T. Y.; Yi, D. K.; Jana, N. R., Functional and Multifunctional Nanoparticles for Bioimaging and Biosensing. *Langmuir* **2009**.
10. Yoon, T. J. Y., K.; Kim, E., Specific Targeting, Cell Sorting, and Bioimaging with Smart Magnetic Silica Core–Shell Nanomaterials**. *Small* **2006,** *2* (2), 209-215.
11. Penn, S. H., L., Nanoparticles for bioanalysis. *Current Opinion in Chemical Biology* **2003,** *7*, 609-615.
12. Brigger, I. D., C., N anoparticles in cancer therapy and diagnosis. *Advanced Drug Delivery Reviews* **2002,** *54*, 631-651.
13. Yezhelyev, M. G., X.; Xing, Y., Emerging use of nanoparticles in diagnosis and treatment of breast cancer. *Lancet Oncol* **2006,** *7*, 657–67.
14. Peer, D. K., J.; Hong, S., Nanocarriers as an emerging platform for cancer therapy. *Nature Nanotechnology* **2007,** *2*, 251-261.
15. H.M., S., Optical measurements in cytometry: Light scattering, extinction, absorption, and fluorescence. *Methods Cell Biol* **2001,** *63*, 107–129; Nu¨sse M, J. l. M., Geido E,, Flow cytometric detection of mitotic cells using the bromodeoxyuridine/DNA technique in combination with 90 degrees and forward scatter measurements. *Cytometry* **1989,** *10*, 312–319.

16. Zucker, R. M. M., E. J. , Detection of TiO2 Nanoparticles in Cells by Flow Cytometry. *Cytometry Part A* **2010,** *77A:* , 677-685; Deng, W. D.-T., K.;, Enhanced Flow Cytometry-Based Bead Immunoassays Using Metal Nanostructures. *Anal. Chem.* **2009,** *81*, 7248–7255.
17. Yguerabide, J., Light-Scattering Submicroscopic Particles as Highly Fluorescent Analogs and Their Use as Tracer Labels in Clinical and Biological Applications. *ANALYTICAL BIOCHEMISTRY* **1998,** *262*, 137–156 ; J., Y., Light-Scattering Submicroscopic Particles as Highly Fluorescent Analogs and Their Use as Tracer Labels in Clinical and Biological Applications
II. Experimental Characterization. *ANALYTICAL BIOCHEMISTRY* **1998,** *262*, 157–176.
18. Jing, Y. M., L. Williams, P, Blood Progenitor Cell Separation From Clinical Leukapheresis Product by Magnetic Nanoparticle Binding and Magnetophoresis. *Biotechnol. Bioeng. 2007;96: 1139–1154.* **2007,** *96*, 1139-1154.
19. McCloskey, K. E. M., L. R., Magnetophoretic Cell Sorting Is a Function of Antibody Binding Capacity. *Biotechnol. Prog.* **2003,** *19*, 899-907; McCloskey, K. E. C., J. J., Magnetic Cell Separation: Characterization of Magnetophoretic Mobility. *Anal. Chem.* **2003,** *75*, 6868-6874.
20. Chalmers J.J, Z. M., Flow through, immunomagnetic cell separation. *Biotechnol Prog* **1998,** *14* (1), 141–148.
21. Williams PS, Z. M., Chalmers JJ., Flow rate optimization for the quadrupole magnetic cell sorter. *Anal Chem* **1999,** *71* (17), 3799–3807.
22. C.L;, T. T. E. M., Purification of hematopoietic stem cells for further biological. *Methods. A Companion to Methods in Enzymology* **1999,** *17*, 202–218.
23. West, J., ENGINEERED NANOMATERIALS FOR BIOPHOTONICS APPLICATIONS: Improving Sensing, Imaging, and Therapeutics. *Annu. Rev. Biomed. Eng. 2003. 5:285–92* **2003,** *5*, 285–92.
24. Englebienne, P., High-throughput screening using the surface plasmon resonance effect of colloidal gold nanoparticles. *Analyst, 2001, 126, 1645–1651* **2001,** *126*, 1645–1651.
25. Vaccaro, D. Y., M. Weinberg, J, Cell Tracking Using Nanoparticles. *J. of Cardiovasc. Trans. Res. (2008) 1:217–220* **2008,** *1*, 217-220; Wuelfing, W. P., Nanometer Gold Clusters Protected by Surface-Bound Monolayers of Thiolated Poly(ethylene glycol) Polymer Electrolyte. *J. Am. Chem. Soc.* **1998,** *120*, 12696-12697.
26. Centrone, A. P., E., The role of nanostructure in the wetting behavior of mixed-monolayer-protected metal nanoparticles. *PNAS* **2008,** *105* (29), 9886–9891.
27. Hussain, S. M. H., K.L, In vitro toxicity of nanoparticles in BRL 3A rat liver cells. *Toxicology in Vitro* **2005,** *19*, 975-983; Sur, I. C., D.; Kahraman, M., Interaction of multi-functional silver nanoparticles with living cells. *Nanotechnology* **2010,** *21*, 175104 (10pp).
28. Gering, J. P.; Quaroni, L.; Chumanov, G., Immobilization of Antibodies on Glass Surfaces through Sugar Residues. *Journal of Colloid and Interface Science* **2002,** *252* (1), 50-56.
29. Heckel, J. C.; Chumanov, G., Depolarized Light Scattering From Single Silver Nanoparticles. *The Journal of Physical Chemistry C* **2011,** *115* (15), 7261-7269.

[30] W. Zhao, E. Pacard, C. Chaix-Bauvais, C. Pichot, and M.A. Brook,. *Colloids and Surfaces A: Physicochemical and Engineering Aspects* (2009), *339,* 26-34.
30. S. A. Maier; M. L. Brongersma; P. G. Kik; Atwater, H. A., *Phys. Rev B* 2002, *65* (19).
31. El-Sayed, M. A., Plasmonic coupling in noble metal nanostructures. *Chemical Physics Letters* 2010, *487*, 153-164.
32. W. Paige Hall; Salome N. Ngatia; Duyne, R. P. V., LSPR Biosensor Signal Enhancement Using Nanoparticle−Antibody Conjugates. *J. Phys. Chem. C* 2011, *115* (5), 1410-1414.
33. Yan, B.; Boriskina, S., *J. Phys. Chem. C* 2011, (115).
34. Haes AJ; Chang L; Klein WL; RP, V. D., Detection of a biomarker for Alzheimer's disease from synthetic and clinical samples using a nanoscale optical biosensor. *J. Am. Chem. Soc* 2005, *127*, 2264-2271.
35. L.C. Wang , N. R. d. T., Electrodeposited copper oxide films: Effect of bath pH on grain orientation and orientation-dependent interfacial behavior. *Thin Solid Films* 2006.